Acoustic Emissions from F-35 Aircraft during Ground Run-Up[*]

Michael M. James[1], Alexandria R. Salton[2], and J. Micah Downing[3]
Blue Ridge Research and Consulting, LLC, Asheville, NC 28801

Kent L. Gee[4], Tracianne B. Neilsen[5], Brent O. Reichman[6]
Brigham Young University, Provo, UT 84602

and

Richard L. McKinley[7], Alan T. Wall[8], Hilary L. Gallagher[9]
Air Force Research Laboratory, Wright-Patterson AFB OH 45433

A multi-organizational effort led by the Air Force Research Laboratory conducted acoustic emissions measurements on the F-35A and F-35B aircraft at Edwards Air Force Base, California in September 2013. These measurements followed American National Standards Institute/Acoustical Society of America S12.75-2012 to collect noise data to support community noise modeling and ground personnel noise exposure assessments. This field study utilized the most spatially extensive measurements of a military jet aircraft to date. In total, the microphone array was composed of 235 unique locations. These locations ranged from radial distances of 3 m outside the shear layer to 1,220 m from the aircraft with angular positions ranging from 0° (aircraft nose) to 160° (edge of the exhaust flow field). The acoustic emissions of the F-35 are presented for engine powers from idle to full augmented power (maximum afterburner). The acoustic emissions are characterized with spatial maps and are discussed in terms of overall and spectral band levels as well as statistical skewness measures. The directivity of the F-35 is described in general and in terms of variations in radial distances and individual spectral bands. Additionally, nonlinear propagation effects are identified and described along the peak radiation region for the range of engine powers.

Nomenclature

ETR	=	engine thrust request, in %
OASPL	=	overall sound pressure level, dB re 20 μPa
OTO	=	one-third octave, dB re 20 μPa
$p(t)$	=	pressure waveform, in Pa
$\partial p/\partial t$	=	time derivative of pressure, in Pa/s
Sk$\{p(t)\}$	=	skewness of pressure, "pressure skewness"
Sk$\{\partial p/\partial t\}$	=	skewness of pressure time derivative, "derivative skewness"

I.   Introduction

The Air Force Research Laboratory (AFRL) led a multi-organization team to perform extensive acoustical measurements on the F-35A and F-35B during static ground run-ups at Edwards Air Force Base (EAFB), California in September 2013. The objective of this field study was to characterize the temporal, spectral, and spatial characteristics of the F-35A and F-35B aircraft. This paper describes the measurements and the initial acoustical emission characterizations of these tactical aircraft. The results provide the required noise data for community and environmental noise studies as well as furnish important measured acoustical data for benchmarking laboratory and computational studies.

Noise generated by high-performance supersonic military aircraft such as the F-35, F-22, and F/A-18E/F are resulting in increased community concerns, noise hazards for ground personnel, and degradation of operational awareness during training and active deployment. Of particular concern is the noise exposure of the flight crew, maintenance personnel, and those aboard aircraft carriers. A better understanding of noise generation mechanisms for jets is required to guide research on effective noise mitigating measures or technologies.[1-4] Although a complete understanding of the entire system, from engine operating state to radiated noise, is difficult to achieve, noise source characterization methodologies have improved the understanding of jet noise. These methodologies include equivalent source models,[5,6] wavepacket models,[7,8] and phased-array[9-11] and holographic[12,13] measurements, have improved the understanding of jet noise generation.

The goals of the current measurements were to a) improve the understanding of noise emissions of the F-35's tactical jet aircraft engines, b) develop directivity data for environmental noise models, and c) examine the acoustic shock characteristics of the waveforms. These measurements followed the recently developed American National Standards Institute/Acoustical Society of America S12.75-2012 tactical aircraft measurement standard. The microphone array was composed of 235 unique locations and organized into multiple elements. These elements included circular arcs, linear arrays parallel to the jet-axis centerline, linear arrays parallel to the jet shear layer, and linear arrays along a radial. The microphone arrays ranged from distances 3.0 m (10 ft) outside the shear layer to 1,220 m (4,000 ft) from the aircraft with angular positions ranging from 0° (aircraft nose) to 160° (approaching the edge of the exhaust flow field).

The results of the F-35 measurements are divided into three main types. First, the acoustic emissions of the F-35 are discussed in terms of spatial maps of overall sound pressure level (OASPL), one-third-octave (OTO) band Sound Pressure Level (SPL), and statistical skewness measures for different engine power conditions. The relationships between OASPL, skewness, and propagation distance and angle are investigated. The pressure waveform skewness (Sk$\{p(t)\}$) has been a long-standing metric of interest within the jet aeroacoustics community.[14,15] [Skewness is a dimensionless normalization of the third central moment of the waveform probability density function (PDF) and characterizes the PDF's asymmetry.] However, McInerny's[16,17] work with rocket noise identified the skewness of the pressure waveform's time derivative (Sk$\{\partial p/\partial t\}$) as a more useful indicator of acoustic shocks and nonlinear propagation. Efforts to predict far-field noise from near-field models and measurements is critical in the investigation of full-scale tactical aircraft jet noise because of the unique effects of nonlinear propagation.[10,1518-26] Recent work has focused on better quantifying this unique behavior.[27-29]

Second, jet noise is highly directional. Thus, the received sound pressure is dependent on observation angle. The directivity of the F-35 static noise is visualized using overall and spectral sound pressure levels, which were measured at angular positions from 0° to 160° around the aircraft, and at five radial distances from 19.1 m (62.5 ft) to 305 m (1,000 ft). This paper highlights trends in the directivity for both measured and normalized sound levels for each ground run-up engine power condition. Lastly, the propagation of the

jet noise along the peak radiation region is examined by observing changes in overall and spectral levels as well as skewness and derivative skewness measures.

II.   Run-up Test Description

The ground run-up measurements for the F-35A and the F-35B were conducted on 5 and 6 September 2013, respectively, at EAFB. The F-35A and F-35B are powered by a Pratt & Whitney F-135 engine with maximum thrust of approximately 191 kN (43,000 lbf).[30] Both aircraft were fastened to the tie down located on Pad 18 as shown in Fig. 1. The terrain around Pad 18 is mostly flat, consisting of the test pad and taxiways surrounded by hard dry lake bed and some desert ground with minimal scrub brush. Thus, most of the array measured noise propagating over fairly rigid and reflective ground surface. The ground run-up measurements were performed between 3:00 and 9:00 AM local time to take advantage of historically favorable atmospheric conditions at EAFB. During this time window, the temperature varied from 19.4°C to 23.1°C, humidity varied from 37.6% to 45.7%, and the average wind speed was 3.3 kts for the F-35A and 1.4 kts for the F-35B. Within these bounds, atmospheric absorption was fairly constant throughout the measurements, which resulted in its variations being negligible when comparing the individual test points.

For the test, measurement points included the entire engine start sequence, specialized maintenance settings, and a full range of steady engine power conditions. This paper focuses on the steady engine power conditions, which were 25%, 50%, 75% (Intermediate), 100% (Military), 130% (Minimum Afterburner) and 150% (Maximum Afterburner) ETR. Each of these engine power settings were repeated five to six times during each six hour test window.

Figure 1. Image of F-35 ground run-up test at Edwards Air Force Base, California.

III.   Acoustic Measurements

A. Measurement Layout

The procedure used to record the F-35A and F-35B ground run-up acoustic emissions conformed to ANSI/ASA S12.75-2012. This data collection represents the most spatially extensive measurements of a military jet aircraft ground run-up to date. Images of F-35 ground run-up measurement layout are shown in Fig. 2. Both aircraft were separately tied down to Pad 18 with microphone array deployed around the port (left) side of the aircraft. The circular microphone array elements were oriented relative to the "microphone array reference point" (MARP) and the heading of the aircraft. The physical position of the MARP was based on a downstream offset from the jet nozzle exit plane and was not changed between each test. However, the relative downstream offset of the MARP was different because of differences in the tie-downs for each variant. The MARP was offset by 6.6 m (21.6 ft) from the F-35A nozzle and by 7.5 m (24.6 ft) from the F-35B nozzle.

The microphone array was composed of thirteen integrated elements: six circular arcs, three linear arrays parallel to the jet-axis centerline, one linear array parallel to the jet shear layer, and three radial arrays in the rear quadrant. The main portion of the array is shown in Figs. 3a and b. The circular arcs were set at radii of 19.1. 28.6, 38.1, 76.2, 152, and 305 m (63, 94, 125, 250, 500, and 1,000 ft). The three parallel arrays were set at lateral offsets of 9.1, 11.5, and 12.8 m (30, 38, and 42 ft). The shear layer arrays were set at offsets of 6.1 and 11.6 m (20 and 38 ft). The radial arrays were at 120°, 135°, and 150°, with

3

microphones extending from the 19.1-m arc to a distance of 1,220 m (4,000 ft). The extended portion of these radial arrays are not shown in Figs. 2a and b. The results shown in this analysis focus on the circular and parallel linear arrays located at distances up to 305 m from the MARP.

Per ANSI S12.75, microphones in the circular arcs were positioned at heights of 1.5 m (5 ft) for distances of 38.1 m and closer, and heights of 3.6, 5.5, and 9.1 m (12, 18, and 30 ft) for distances of 76.2, 152, and 305 m, respectively. For the 9.1 and 12.8 m offset parallel arrays, the microphones were set at 0.9 and 1.5 m (3 and 5 ft), respectively. For the 11.5 m offset parallel array, the microphones were placed in inverted mounts, which provided an effective measurement height of 0 m. For the radial arrays, the microphones were placed at heights from 1.5 m at the closest locations, increasing gradually to heights of 9.1 m (30 ft) for the microphones 305 m and out. In addition, vertical microphone arrays were placed at the 135° radial locations of 610 m (2000 ft) and 1220 m, with microphones from 0 m to 30.5 m (100 ft) in height. The pressure microphones were oriented for nominally grazing incidence. The free-field microphones were pointed toward the MARP.

Multiple data acquisition systems were operated simultaneously by the five participating organizations: AFRL, Blue Ridge Research and Consulting, LLC (BRRC), Brigham Young University (BYU), Wyle Laboratories (Wyle), and Naval Air Systems Command (NAVAIR). A total of 340 microphones were deployed over the 235 locations to provided redundancy for the more crucial locations. All microphones and data acquisition systems conformed to the guidelines in ANSI/ASA S12.75-2012.

B. Instrumentation

The pressure time waveforms from the microphones at distances of 76.2 m and closer to the MARP were recorded on a multi-channel data acquisition system built on the National Instruments (NI) PXI platform. The PXI chassis included eleven 4-channel NI PXI-4462 and two 16-channel NI PXI-4496 DSA boards with simultaneous sampling to ensure correct phasing of all recorded channels. The DSA modules are ideal for making precision microphone measurements since they have 24-bit analog inputs per module and Integrated Electronic Piezoelectric (IEPE) constant current signal conditioning. The modules deliver over 114 dB of dynamic range and simultaneous sampling on all channels at rates up to 204.8 kS/s. Digitized data from all channels were streamed over a single optical cable to a high powered Intel processor based Microsoft Windows 7 controller. The controller has four solid state drives (SSD), which have increased vibration tolerance and superior write speed. The SSDs are deployed in a RAID 10 configuration, which is optimal for mission critical applications as the data are striped across two SSDs for increased performance and mirrored across two SSDs for redundancy in case of a drive failure. For measurement locations in high amplitude pressures, 6.35 mm (¼ inch) G.R.A.S. 46BG, 46BD, and 46BE microphones were paired with a 26CB preamplifier. These microphone-preamplifier pairings have a minimum frequency response of 6.5 Hz – 90 kHz. The constant current preamplifiers were powered by the IEPE conditioning onboard the data acquisition system.

The time waveforms from the microphones at distances of 152 and 305 m from the MARP were collected on 8-channel NI PXI-4472B DSA boards with simultaneous sampling, for all but the 0° – 40° and 60° – 80° 305m locations. The sound pressure measurements were made with G.R.A.S. 40BH, Brüel & Kjær 4190, and Brüel & Kjær 4191 microphones. The 0° – 40° and 60° – 80°, 305 m waveforms were recorded with Larson Davis 831 sound level meters, capable of recording time-history Waveform Audio File Format (wav) files. IRIG-B time code was simultaneously recorded along with the pressure time signatures across all array elements throughout the duration of the test to allow for synchronization of the pressure, engine, and weather data. In addition to the aircraft noise recordings, calibration tones and ambient sound levels were recorded before and after the test measurements.
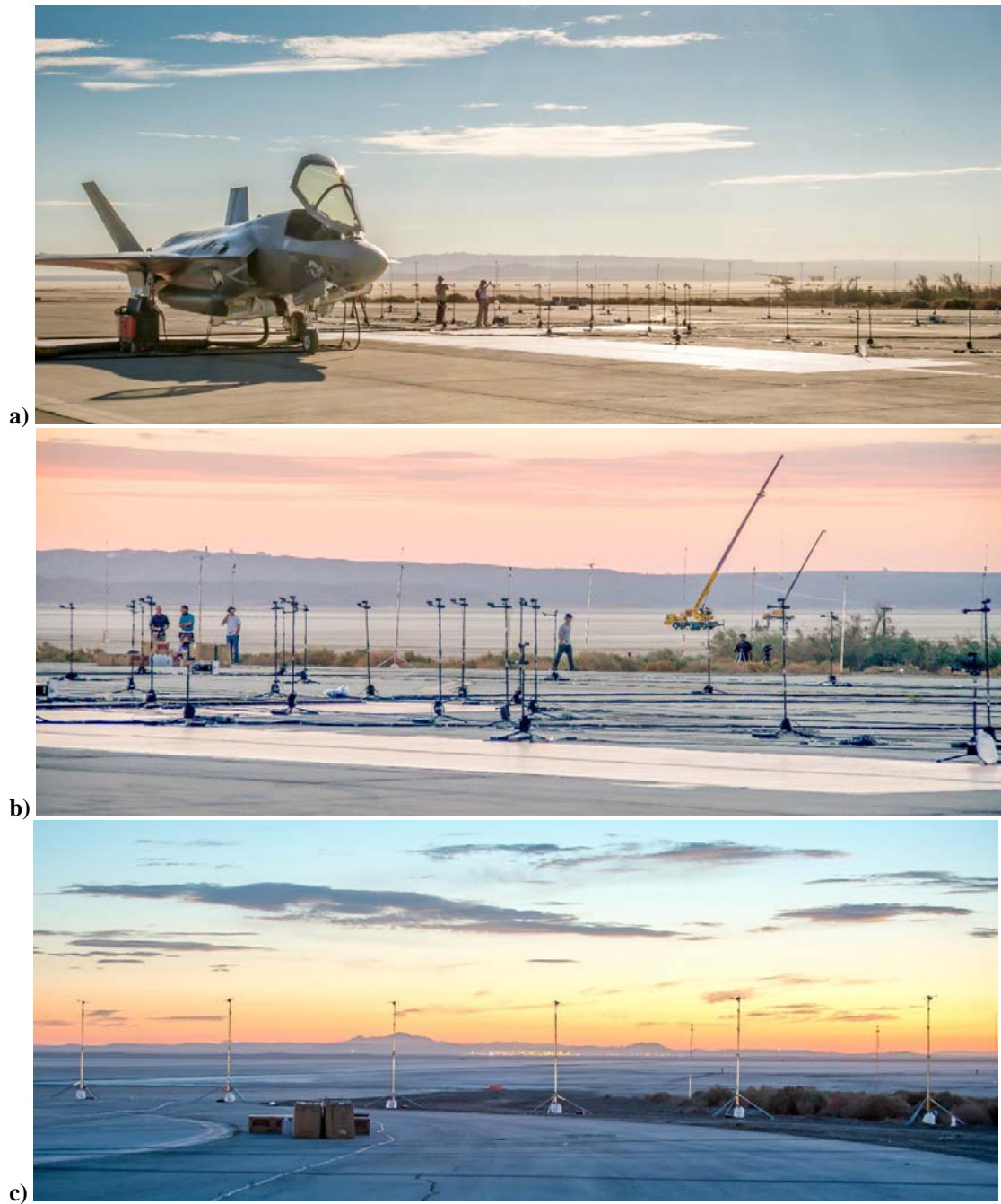
American Institute of Aeronautics and Astronautics

Figure 2. Images of F-35 ground run-up measurement layout at Edwards Air Force Base, California: a) aircraft shown in reference to microphone arrays, b) microphone arrays with 610 and 1,220 m cranes in the distance, and c) aft-quadrant of the 76.2 m microphone array with the 152 and 305 m arrays in the distance.

American Institute of Aeronautics and Astronautics
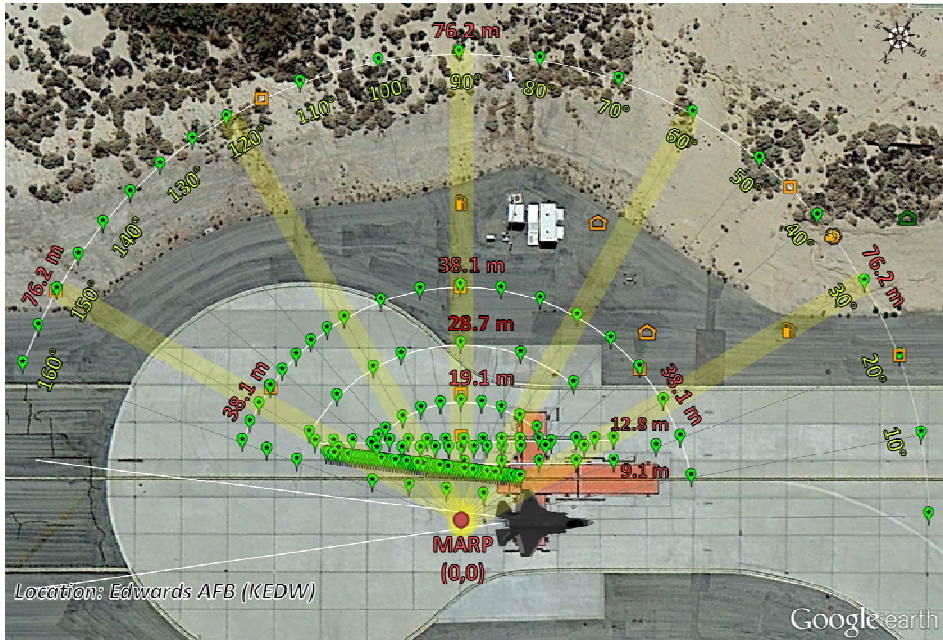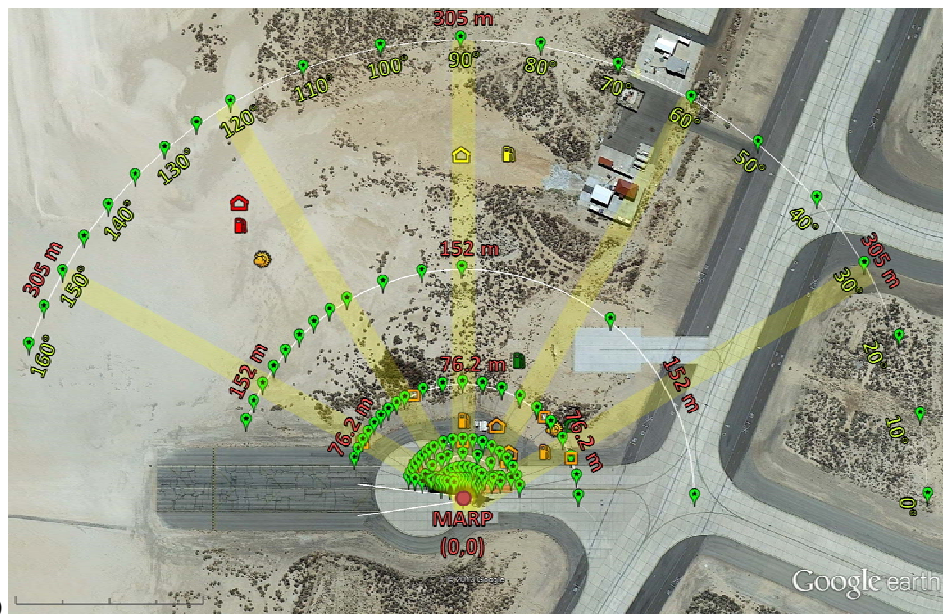
Figure 3. F-35 acoustic measurement layout, extending to a) 76.2 m and b) 305 m at Edwards Air Force Base Pad 18.

IV. Analysis

This section describes the post-processing of the recorded waveforms and generation of the final acoustical dataset. The processing initially involved the generation of detailed narrow band spectra and pressure time histories for detailed data inspection and removal of spurious data. After the data inspection, overall levels and OTO band spectra were generated for further analysis of the F-35 noise emissions.

A. Time and Spectral Analysis

For each run-up event, data were recorded by multiple organizations operating multiple data acquisition systems. During post-processing, best efforts were made to ensure each waveform had the same start and stop times, with appropriate signal propagation delay times factored in for the distant arrays. Trimming the recording samples to the same length (30 seconds or greater) ensured that time-weighted metrics were computed on a consistent basis. Spectral analysis, conforming to ANSI/ASA S12.75-2012, was performed on the waveforms to obtain average spectra for each recorded sample. Products from this analysis include time history and average power spectral density (PSD) plots; examples are shown in Figs. 4a and b, respectively. The PSD data were used to generate OTO band SPL plots, examples of which are shown in Figs. 4c and d, corresponding to the time history and average OTO band plots, respectively.
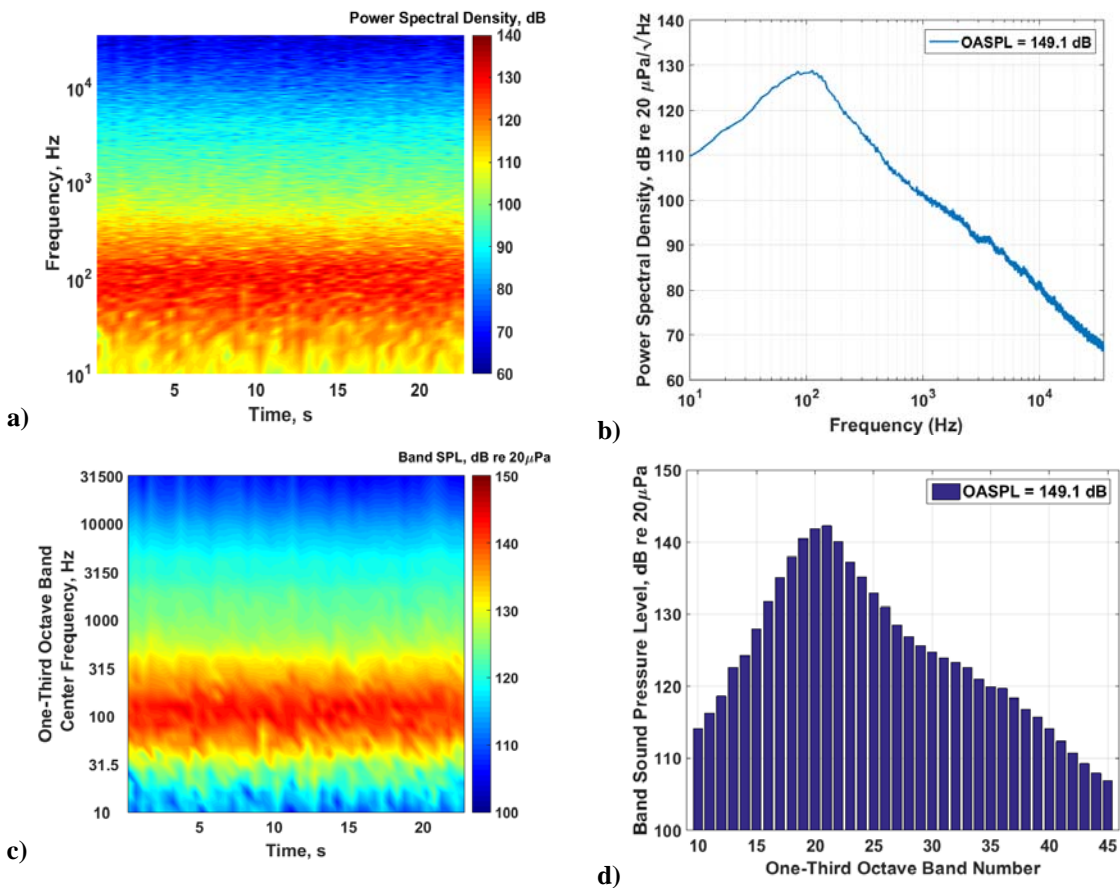

Figure 4. Spectral analysis for 150% ETR (maximum afterburner): a) PSD time history, b) overall PSD, c) OTO band time history, and d) overall OTO band.

American Institute of Aeronautics and Astronautics

B. Microphone and Standard Day Corrections

Two microphone corrections were applied to the recorded data during post processing. The first correction is a frequency response correction based on the electrostatic actuator response for each individual microphone, which was provided by the manufacturers. The second is an angle of incidence correction, which is the same for each size of microphone, and it was also provided by the manufacturers. The angle of incidence was known for each microphone based on its orientation, with respect to the MARP, during the test.

C. Determination of Median Quantities

To determine a representative overall level at each microphone position, the median sound level value was determined from the sample of 5 to 6 recordings of each test condition. The acoustic metrics processed in this manner include the flat-weighted and A-weighted OASPL. Figure 5a shows the sound level plots for one microphone position and a sample of five 150% ETR events. For this test condition, the median flat-weighted OASPL was 149.0 dB. Figure 5b shows the median sound level ± two standard deviations at each OTO band center frequency. The standard deviation of the OASPL among the runs is generally less than 1 dB at all measurement points except for those in the vicinity of the shear layer. Measurement locations far aft of the nozzle and along the 155° and 160° radials exhibited larger deviations because of the variability of jet flow field interactions with the surrounding quiescent air from small changes in the wind direction.
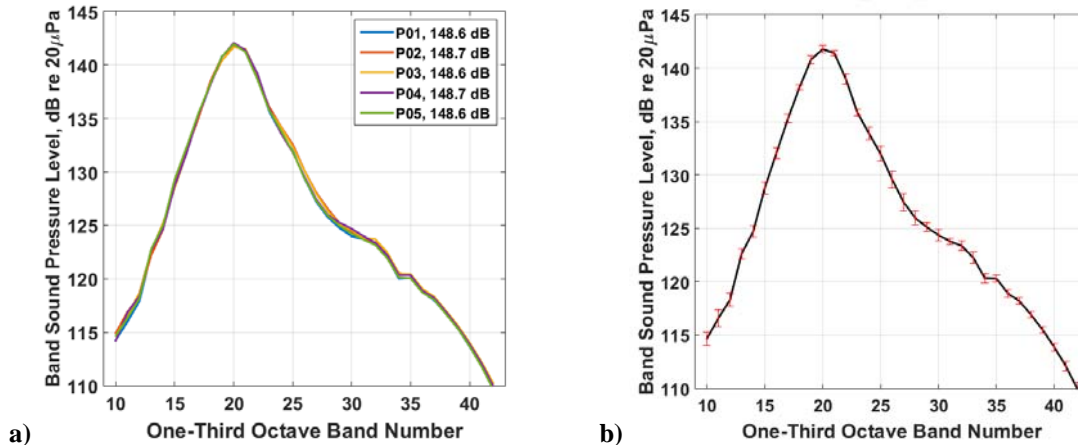

Figure 5. Determination of the median sound level from a sample of five 150% ETR events: a) sound levels for events P01-P05, b) median +/- one standard deviation of the five events.

American Institute of Aeronautics and Astronautics

V.   Results

The following results highlight the acoustic emissions from the F-35A and F-35B aircraft for engine power conditions ranging from 25% to 150% ETR during ground run-up operations. The OASPL, pressure skewness, derivative skewness, and OTO band SPL spatial maps spanning angular positions from 0° to 160° and distance out to 305 m are presented. Additionally, directivity based on OASPL and OTO band SPL are shown for a range of radial distances and compared as a function of engine power condition, OTO band center frequency, and propagation distance. Finally, OASPL, OTO band SPL, skewness, and derivative skewness along the peak radiation angle of each power condition are discussed in terms of sound propagation. For brevity, acoustic emission results concentrate on the F-35B data, but the F-35A results exhibit similar trends.

A. Spatial Maps

1. Overall Sound Pressure Level

The present work builds on analyses involving previous measurements of the F-35AA[27-29, 32] and considers OASPL for 25%, 75%, 100%, and 130% ETR to illustrate the differences in acoustic emission from low to high-power engine conditions. The spatial maps of OASPL from the MARP position out to 76.2 m and 305 m are presented side by side in Figs. 6 and 7, respectively. This split allows both near-field and far-field features to be observed. The data are represented as a spatial color map, with contours overlaid on the color map to identify lines of equal level. The gradients between measured microphone locations were evaluated based on a cubic interpolation. An examination of the locations of the peak OASPLs at 305 m (Fig. 7a through d) shows that the maximum directivity angle shifts from about 150° to 125° as power increases from 25% to 130% ETR.

Care must be taken in the definition of far-field directivity for a highly heated, supersonic jet. At a distance of 305 m or approximately 300 nozzle diameters, the source can be considered relatively compact and could be treated as occurring at the nozzle exit. However, as the distance from the measurement array to the jet decreases, the identification of the actual source location is required to define accurately the radiation angles. For example, for 75% ETR in Fig. 6b, the maximum radiation lobe at 76.2 m occurs in the 135° region, when the angle is referenced to the MARP. However, if the nozzle exit plane were utilized as the reference point, then the maximum radiation would be shifted approximately 5° aft to 140°. The selection of a MARP location 7 to 8 nozzle diameters aft of the nozzle has been used in prior jet measurements involving the F-35AA-1[27-29,31,32] and the F-22A.[22] The F-22A analysis demonstrated that measured waveform segments along the maximum radiation direction from 23-305 m, as referenced from the MARP, were highly correlated via visual inspection. Both holographic[13] and phased-array[11] source reconstructions of the F-22A operating at Military power placed source maxima between 6 and 12 nozzle diameters for respective frequencies between 1000 Hz and 50 Hz, respectively; the same frequencies for Maximum Afterburner were placed between 8 and 15 nozzle diameters.
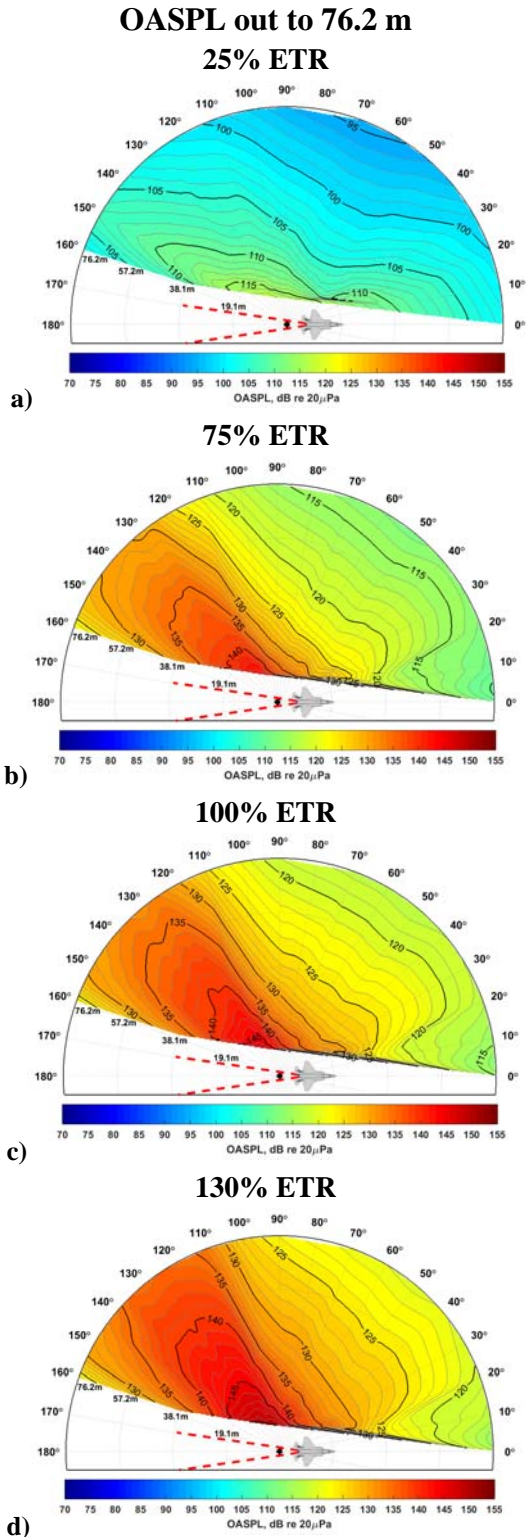
American Institute of Aeronautics and Astronautics

OASPL out to 76.2 m

OASPL out to 305 m

25% ETR

25% ETR

a)

a)

75% ETR

75% ETR

b)

b)

100% ETR

100% ETR

c)

c)

130% ETR

130% ETR

d)

d)

Figure 6. OASPL of an F-35B at locations from the MARP out to 76.2 m for a) 25% ETR, b) 75% ETR, c) 100% ETR, and d) 130%.

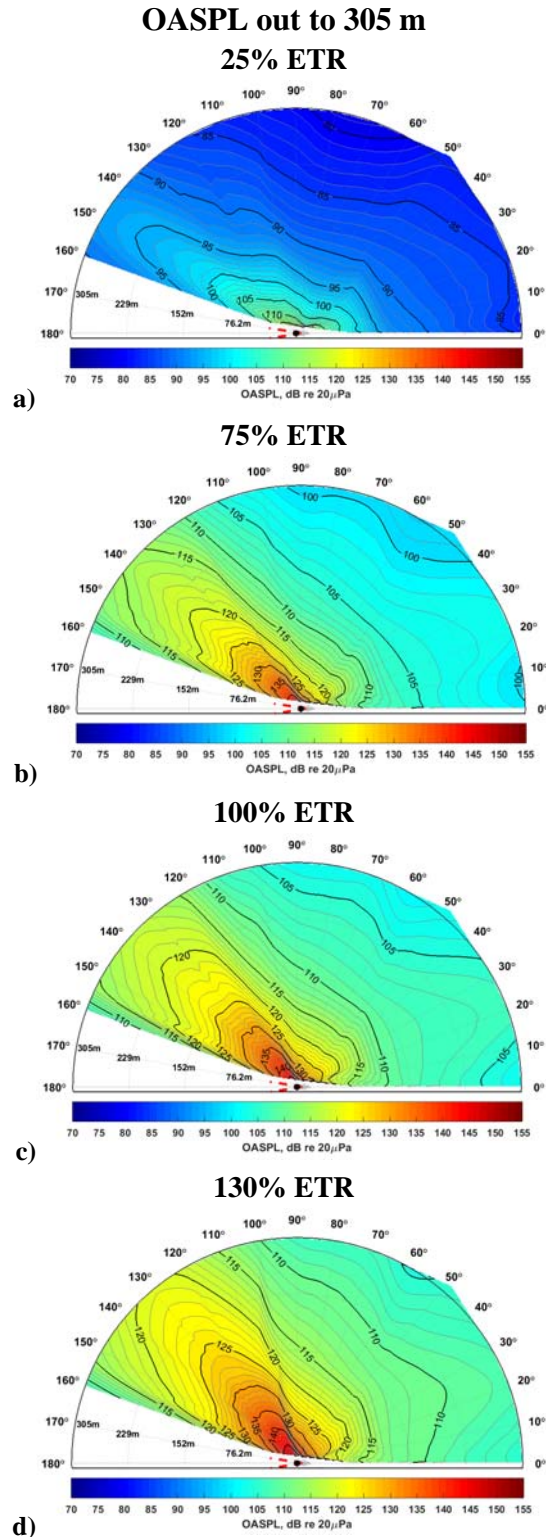**Figure 7. OASPL of an F-35B at locations from the MARP out to 305 m for a) 25% ETR, b) 75% ETR, c) 100% ETR, and d) 130%.**

10
American Institute of Aeronautics and Astronautics

2. Skewness Metrics

The spatial maps for $\text{Sk}\{p(t)\}$ and $\text{Sk}\{\partial p/\partial t\}$ for engine power conditions 25%, 75%, 100%, and 130% ETR are provided to highlight trends in the measured data. The $\text{Sk}\{p(t)\}$ and $\text{Sk}\{\partial p/\partial t\}$ spatial contours out to 305 m are shown in Figs. 8 and 9, respectively. These provide insight into the spatial properties of the skewness of the acoustic pressure waveform and its time derivative with greater spatial resolution and measurement aperture than previous full-scale measurements.[27,29] In Fig. 8a, the 25% ETR pressure skewness values range between approximately 0.0 and 0.2. With an increase in engine power to 75% ETR, shown in Fig. 8b, the pressure skewness values range between approximately 0.0 and 0.5. For this engine power, $\text{Sk}\{p(t)\}$ reaches a maximum along the 125° radial, which is approximately 15° upstream of the OASPL directivity lobe. The fact that $\text{Sk}\{p(t)\}$ peaks at directivity angles upstream of the OASPL agrees with the results in Refs. 27 and 29. As the engine power is increased to 130% ETR, shown in Fig. 8d, the values of skewness increase to above 0.8, and the angle of the maximum decreases to 110˚. However, the values exceed 0.4 over an angular aperture from about 100-120°, which is larger than lower engine powers.

Figure 9 provides the results for $\text{Sk}\{\partial p/\partial t\}$ as a function of engine power. For the 25% engine power in Fig. 9a, $\text{Sk}\{\partial p/\partial t\}$ is approximately zero at all measured locations, indicating no evidence of the presence of weak acoustic shocks. For the engine power of 75% ETR, as shown in Fig. 9b, $\text{Sk}\{\partial p/\partial t\}$ increases as the noise propagates away from the source, reaches a maximum above 16 between approximately 76.2 to 152 m, then decays away. This increase occurs along a relatively narrow angle near 135°. As the engine power condition is increased to 130% ETR, shown in Fig. 9d, $\text{Sk}\{\partial p/\partial t\}$ exceeds values of 23 along the angle of 130° from a distance of approximately 36 to 210 m, after which it decreases.

A potential explanation for a systematic increase in $\text{Sk}\{\partial p/\partial t\}$ values as the noise propagates away from the jet along the maximum radiation direction is nonlinear waveform steepening.[27-29] Although the low engine power condition of 25% ETR has no appreciable $\text{Sk}\{\partial p/\partial t\}$ values and thus likely undergoes little nonlinear steepening, all of the higher engine power conditions show a peak in $\text{Sk}\{\partial p/\partial t\}$, just outside 76.2 m. After this maximum, the shock amplitudes decay which leads to decreases in $\text{Sk}\{\partial p/\partial t\}$. Also, the width of the $\text{Sk}\{\partial p/\partial t\}$ lobe increases with propagation, which suggests nonlinear propagation over a broad angular range.

A more thorough investigation of the measured spectra is required to show the effect of nonlinear steepening, which will be explored later in this paper. This analysis is the first for full-scale jet data that has a sufficiently large measurement spatial extent and resolution to show the clear growth and decay of $\text{Sk}\{\partial p/\partial t\}$. This dataset will enable further understanding of the connection between values of $\text{Sk}\{\partial p/\partial t\}$ and weak-shock-like behavior, including shock formation and thickening.
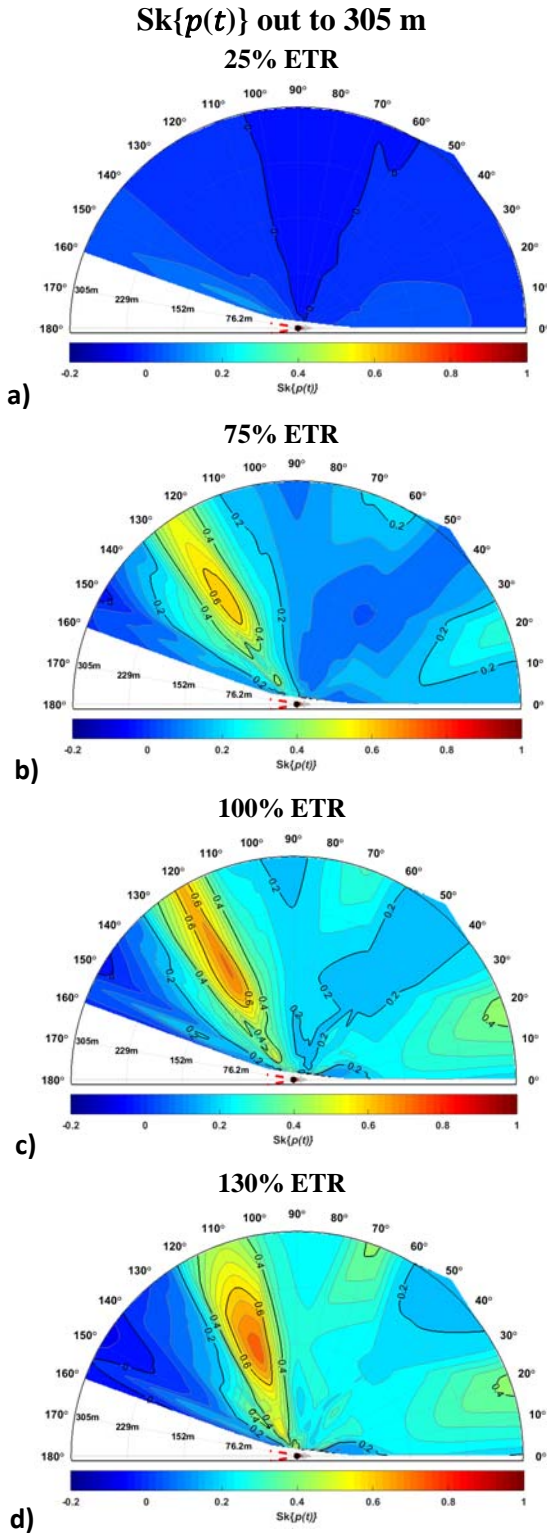
Sk{$p(t)$} out to 305 m

a)

b)

c)

d)

Figure 8. Skewness of pressure, Sk{$p(t)$}, of an F-35B at locations from the MARP out to 305 m for a) 25% ETR, b) 75% ETR, c) 100% ETR, and d) 130% ETR.
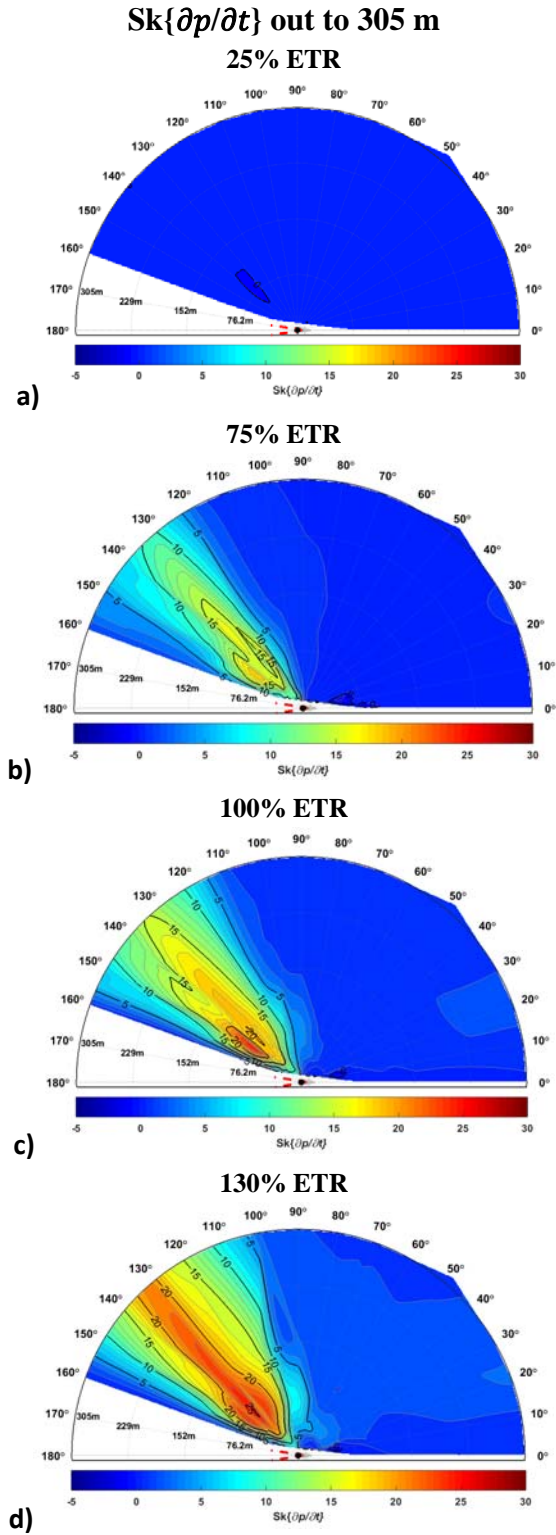
Sk{$\partial p/\partial t$} out to 305 m

a)

b)

c)

d)

Figure 9. Skewness of pressure time derivative, Sk{$\partial p/\partial t$}, of an F-35B at locations from the MARP out to 305 m for a) 25% ETR, b) 75% ETR, c) 100% ETR, and d) 130% ETR.

3. One-Third Octave Band Sound Pressure Level

Spatial OTO band SPL maps ranging from the MARP position out to 76.2 m and angular positions from 0° to 160° are shown in Fig. 10 for 75% ETR. Figure 10a through f includes select OTO band center frequencies from 10 to 10,000 Hz. A clear shift is observed in the maximum directivity angles from approximately 160° to 130° as the frequency increases from 10 Hz to 10,000 Hz . The 10-Hz OTO band apparent source region, as shown in Fig. 10a, appears to be extended in length and originating well downstream of the MARP. Moving up in frequency to 100 Hz in Fig. 10c and 315 Hz in Fig. 10d, which are within the maximum frequency content for 75% ETR, the apparent source origination appears to be near the MARP location point. At 10,000 Hz the apparent source origin shifts farther upstream towards the nozzle exit plane. The OTO band SPLs for 130% ETR engine power condition are shown in Fig. 11, and similar trends hold true for this engine power. The maximum directivity angles shift from approximately 155° to 115° as the OTO band center frequency increases from 10 Hz to 10,000 Hz.
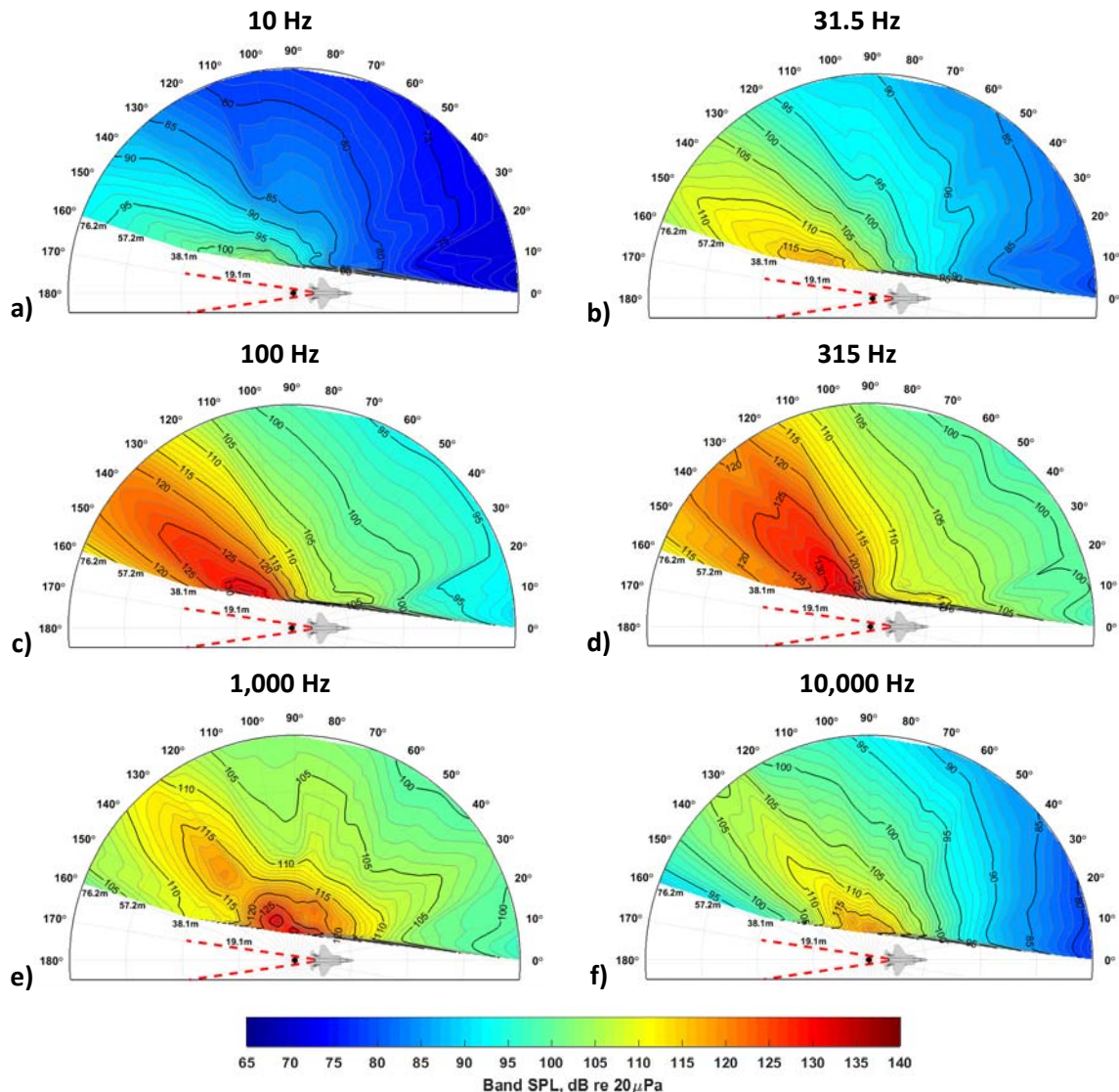

Figure 10. OTO band SPL of an F-35B at 75% ETR, at locations from the MARP up to 76.2 m for a) 10 Hz, b) 31.5 Hz, c) 100 Hz, d) 315 Hz, e) 1,000 Hz, and f) 10,000 Hz.
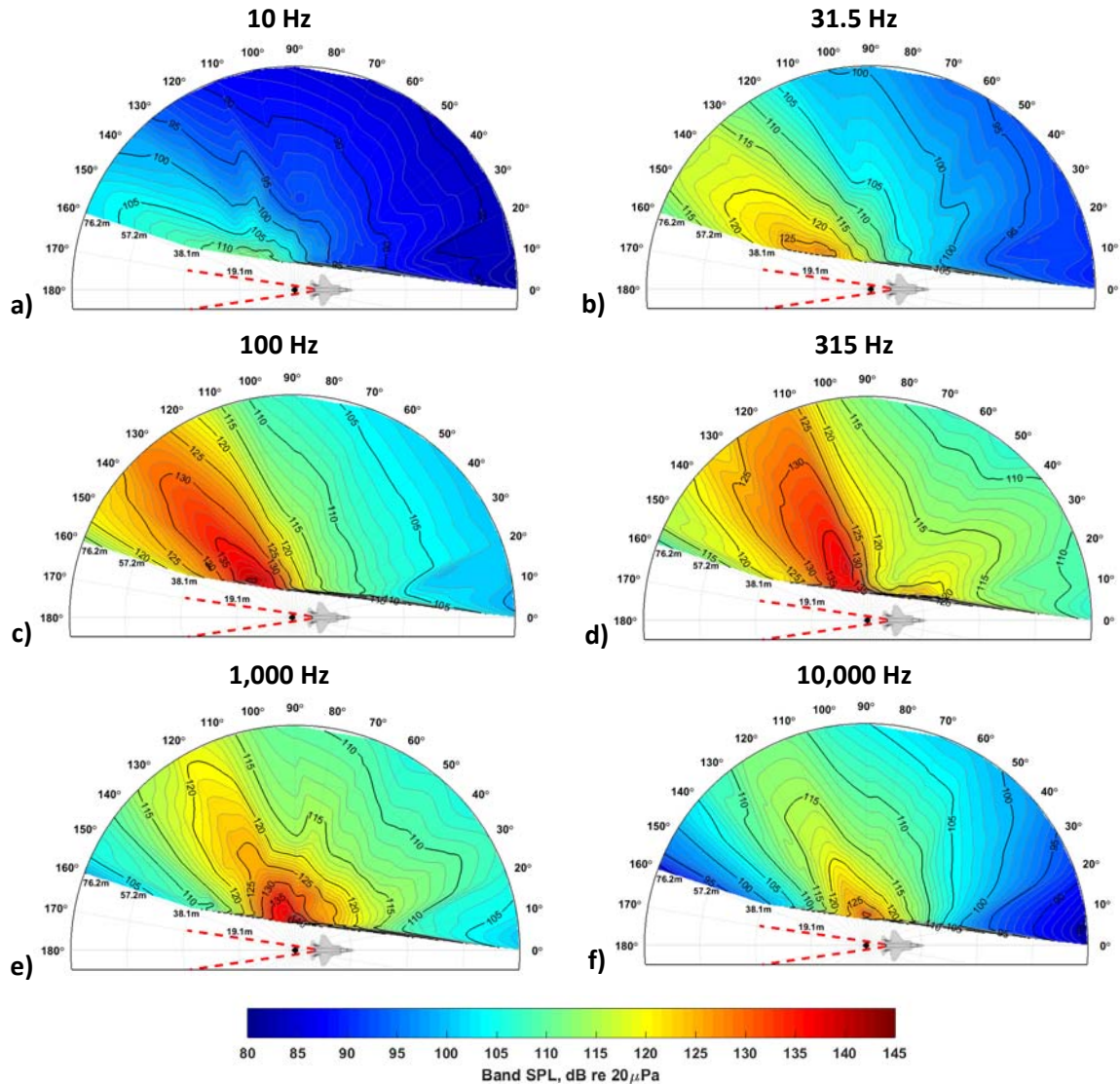
Figure 11. OTO band SPL of an F-35B at 130% ETR, at locations from the MARP up to 76.2 m for a) 10 Hz, b) 100 Hz, c) 315 Hz, d) 1,000 Hz, and e) 10,000 Hz.

Along with these general trends observed in the OTO band sound levels, other effects are important to note in the OTO data. First, the 1,000 Hz map for 75% ETR in Fig. 10e shows interference nulls at approximately 10 and 28 m, particularly along the maximum radiation lobe. The locations of these nulls reasonably align with the multipath interference of a monopole above a rigid plane for the same measurement geometry. As the engine power is increased to 130% ETR, Fig. 11e, the nulls, if present, are not nearly as pronounced. This reduction in the interference null can be attributed to increases in the source distribution and flow entrainment. The source distribution for the afterburner case is appreciably more extended as the core length is expanded and more ambient air is entrained into the jet flow near the shear layer. These changes result in only partial coherence between the direct and reflected fields[33]. Second, at 1,000 Hz for 75% ETR and 315 and 1,000 Hz for 130% ETR, radiation lobes are observed in the upstream direction. The physical process generating these forward lobes needs further investigation. Potential mechanisms are broadband-shock associated noise originating in the aft region or engine inlet noise. Third, a notable dual principal radiation lobe exists for 315 Hz for 75% ETR (Fig. 10d) and to a lesser extend for 130% ETR (Fig. 11d). This dual lobe has been the subject of studies related to the F-22 at military and afterburner engine conditions[34]-[37]. The observance of the lobe at a lower engine power for the F-35B than has been seen for other aircraft is noteworthy and should be motivation for further study.

14
American Institute of Aeronautics and Astronautics

B. Directivity

1. Overall Sound Pressure Level

A fundamental objective of this measurement program is the development of run-up directivity datasets for environmental noise models and as benchmarks for laboratory-scale data and numerical jet noise models. This dataset includes OASPL and OTO band SPL at each angular measurement position (0° to 160°) around the aircraft, measured at a distance of 76.2 m from the MARP, for all engine power conditions (25% through 150% ETR) measured. Although the measurement array had a fixed origin, in reality, the apparent source origin of each source varies with engine power and frequency, as demonstrated for high-power full-scale jet noise using various methods.[38-40] The directivity patterns based on OASPL for the F-35B are depicted in Fig. 12. The directivity as the engine power increases from 25% to 150% ETR shows an increase in the OASPL and a clear shift in the maximum directivity angles from approximately 150° to 120°. Additionally, the results for the F-35A ground run-up directivity patterns are essentially equivalent as shown in Fig. 13. Because the maximum directivity angles for the two Afterburner conditions occur as far forward as 120˚, expansion of ANSI S12.75 is recommended to include the addition of 115° and 105° microphone locations to the radial arrays to ensure the maximum acoustic radiation region is captured with the finer angular resolution.
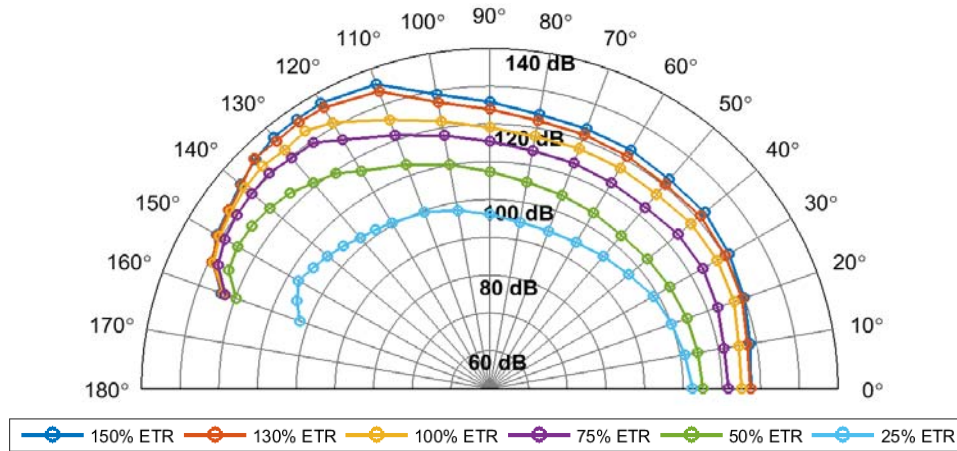

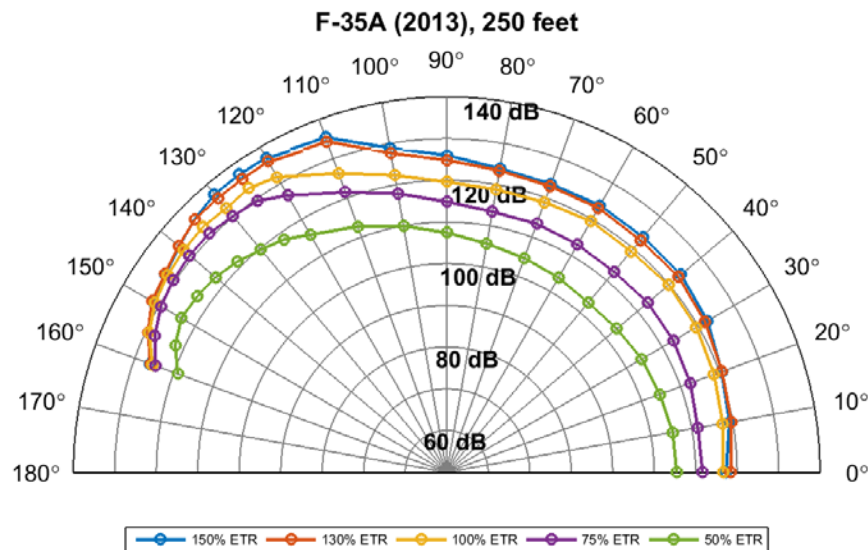Figure 12. F-35B directivity based on OASPL at a distance of 76.2 m from the MARP.

Figure 13. F-35A directivity based on OASPL at a distance of 76.2 m from the MARP.

2. One-Third Octave Band Sound Pressure Level

The directivity of the F-35B at 76.2 m is further broken down in terms of select OTO bands and several engine powers. The OASPL and OTO band SPL for 10, 31.5, 100, 315, 1,000, and 10,000 Hz are shown over a range of engine power conditions from 25% to 150% ETR, in Fig. 14a through f. Representation of the data in this manner allows clear visualization of the frequency regions that contribute most to the level and shape of the OASPL-based directivity. At 25% ETR, shown in Fig. 14a, the 100 Hz band contributes significantly to the level and shape of the OASPL. Moving up in engine power (50% to 150% ETR), Fig. 12b through f, the OASPL in the maximum radiation region (110° to 150°) is dominated by the 100 to 315 Hz frequency region. Upstream and to the sideline (0° to 100°) of the MARP the most significant contribution to the OASPL is the 315 to 1,000 Hz frequency region.
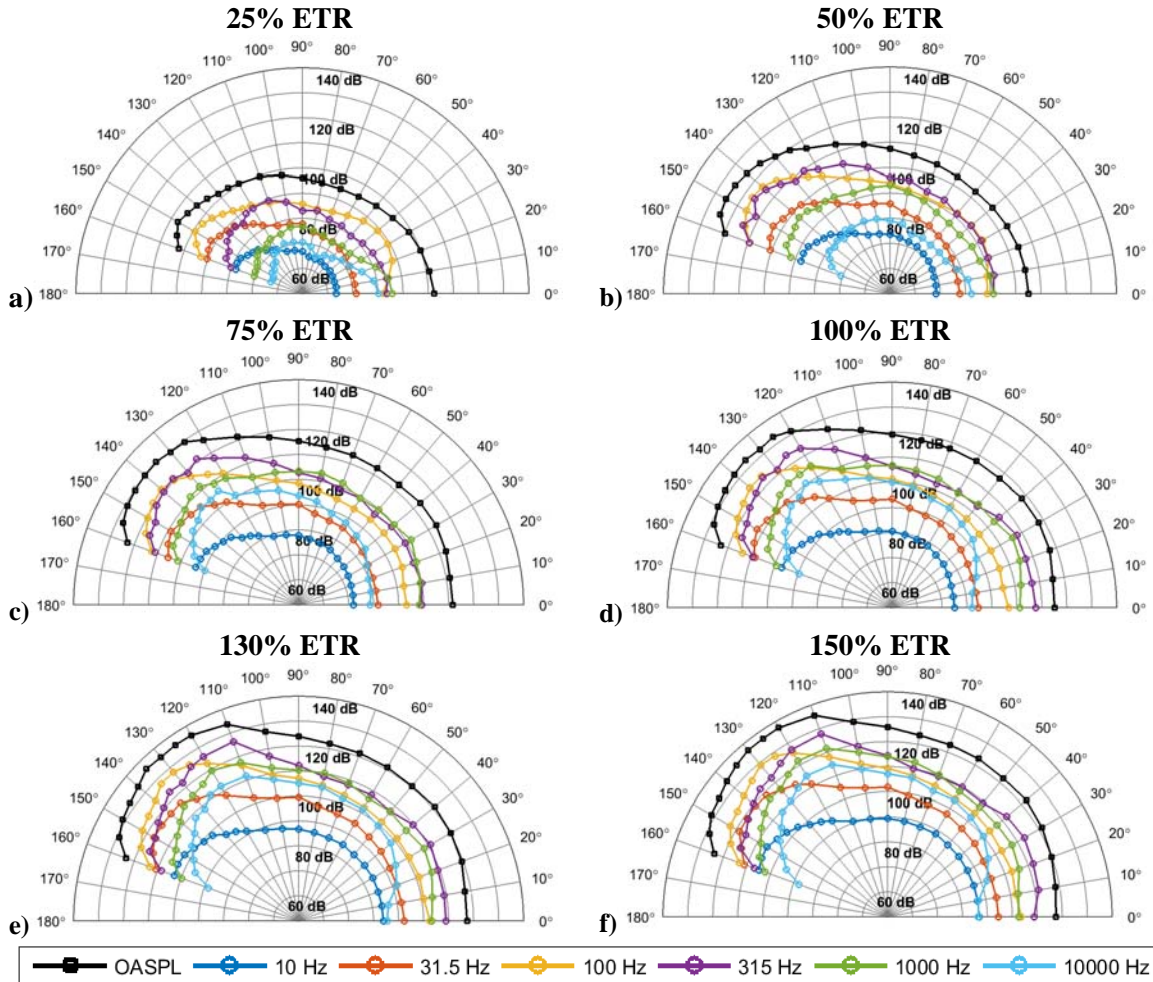

Figure 14. F-35B directivity at 76.2 m based on OASPL and 10, 31.5, 100, 315, 1,000, and 10,000 Hz OTO band SPL for a) 25% ETR, b) 50% ETR, c) 75% ETR, d) 100% ETR, e) 130% ETR, and f) 150% ETR.

Next, the same data are regrouped by OTO band center frequencies to show the changes resulting from engine power conditions as shown in Fig. 15a through f. This grouping facilitates comparison of OTO band SPL directivity as a function of engine power. At 10 and 31.5 Hz, shown in Figs. 15a and b, respectively, the shape of the directivity patterns are consistent across engine power conditions, with levels uniformly increasing as engine power is increased from 25% to 150% ETR. This observation is remarkable because the jet noise exhibits a form of thrust-related scalability for these low frequencies even though the jet noise source is dramatically different in terms of velocity and temperature differences between 25% and 150% ETR engine power conditions. For 100 Hz, shown in Fig. 15c, the levels of engine powers 75% to 150% ETR at angles larger than 140° converge to within about a 10-dB range, while the levels vary more as a function of engine power forward of this angle. As frequency increases toward 10,000 Hz in Fig. 15c through f, the curves in this aft region converge further. The convergence is less than a 10-dB aft of 120° and tightens to a 1-dB range at 160° in Fig. 15f. The physical rationale behind this observation remains to be investigated, but suggests that the noise source in this angular region beyond the principal (Mach wave) radiation lobe approaches relatively invariant behavior. Directly in front of the aircraft (0°) and at 10,000 Hz (shown in Fig. 15f), the OTO band SPL converges over all power conditions, indicating the levels at this frequency are likely driven by inlet noise. At 1,000 and 10,000 Hz, Figs. 15e and f, respectively the radiation for 25% ETR is directed toward the sideline, as well as far forward, but by 50% ETR the peak directivity corresponds roughly with that of the OASPL. Finally at 10 Hz, the maximum directivity angle is about 160° for all engine powers shown in Fig. 15a. As frequency is increased, the maximum directivity region shifts forward, reaching between 125° and 110° in Fig. 15f.
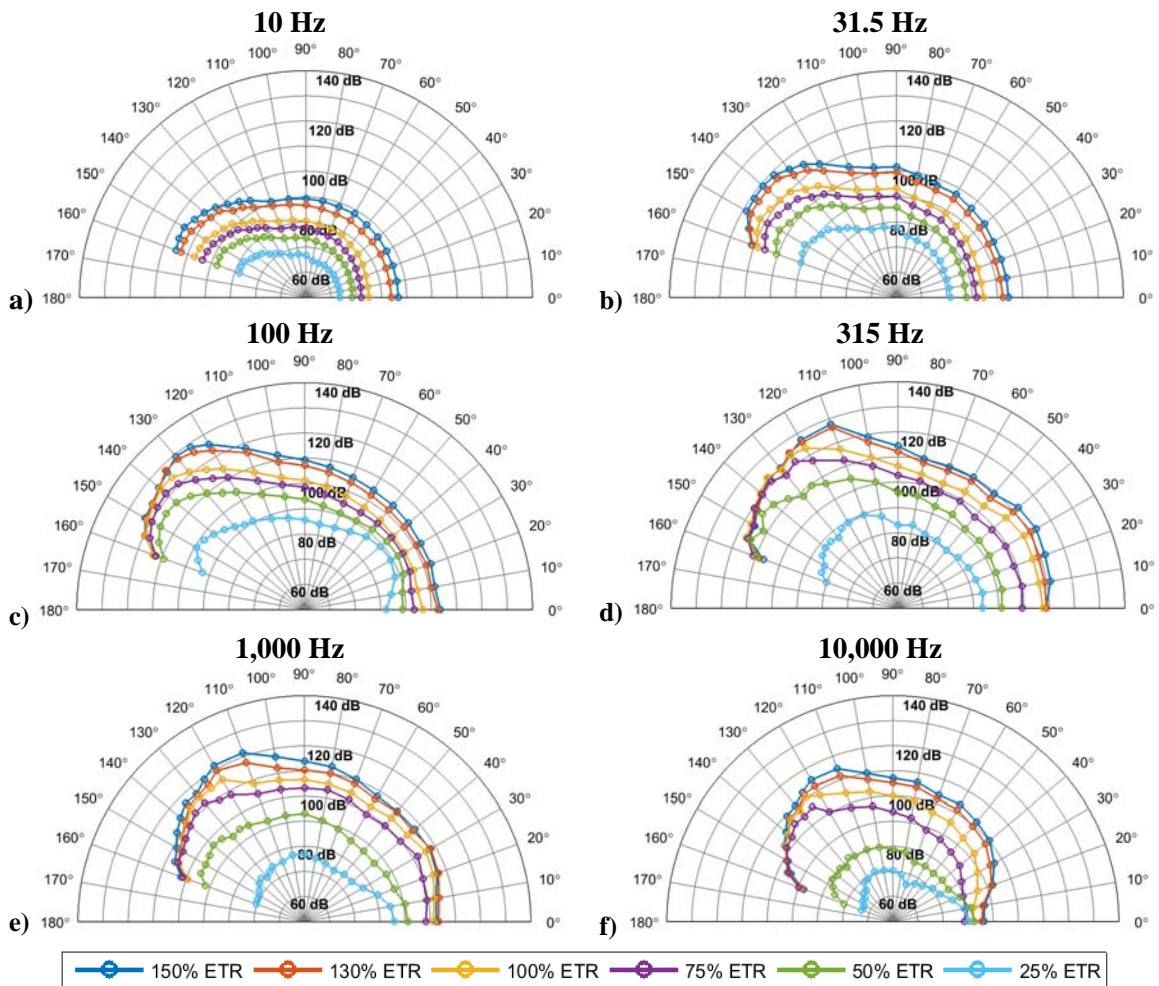

Figure 15. F-35B directivity at 76.2 m based on OTO band SPL for 25%, 50%, 75%, 100%, 130%, and 150% ETR for a) 10 Hz b) 31.5 Hz, c) 100 Hz, d) 315 Hz, e) 1,000 Hz, and f) 10,000 Hz.

3. Overall Sound Pressure Level Normalized by Distance

The OASPL at distances of 19.1, 28.6, 38.1, 76.2, 152, and 305 m from the MARP are normalized to a distance of 1 m (based on a spherical spreading factor) to investigate changes in the directivity pattern over a range of propagation distances. The levels for each figure were then adjusted relative to the maximum OASPL over all distances and angles. No adjustments are made for atmospheric absorption, nonlinear propagation effects, or ground interference. The F-35B directivity based on this normalized OASPL is shown for 25% to 150% ETR in Fig. 16a through f. (Note, the angular resolution of the front half of the 152.4 m arc is limited to 0°, 50°, and 90°.) In Fig. 16a, the 25% relative directivity curves of all the arcs collapse to within 3 dB or less for maximum radiation angles and in the 40˚-50˚ direction. These same angles are dominated by the 100 Hz OTO band, as shown in Fig. 14a. However, in the sideline and forward angles, which are dominated by the higher frequencies of 315 and 1000 Hz, normalized level tends to decrease with distance from the MARP. Thus, the angles where higher frequencies dominate are likely subject to effects other than spherical spreading, such as atmospheric absorption. However, care must be taken in the interpretation of these results, because measurements beyond 76.2 m were complicated by terrain variations beyond the ANSI S12-75 limits (see Fig.3b).

Indeed, according to Fig. 16, the terrain variations (dominated by scrub brush) appear to be highest in the directions from about 50˚ to 120˚, and to a lesser extent, as far aft as 150˚. The propagation paths in the forward direction occur mainly over taxiways. The variations in normalized directivity for most engine powers and angles in Fig. 16 follow the trends of the terrain; relative levels in the directions from 50˚ to 120˚ decrease by about 5 to 10 dB with distance, they collapse to within about 5 dB at angles larger than 120˚, and they are almost fully collapsed to within about 1 dB in the forward direction.

Additional propagation effects, whether they are terrain, atmospheric absorption, or other factors, affect the 152 and 305 m directivities the most. Of particular note is the consistency in levels from 19.1 to 76.2 m for all engine powers in Fig. 16b, which typically collapse to within 2 dB and never exceed 4 dB, indicating that far-field directivity based on OASPL can be estimated relatively well using measurement distances as close as 19.1 m to the MARP. The measurements at 152 m and beyond require more analysis to account for the additional *in situ* effects before they can be accurately compared in this manner.
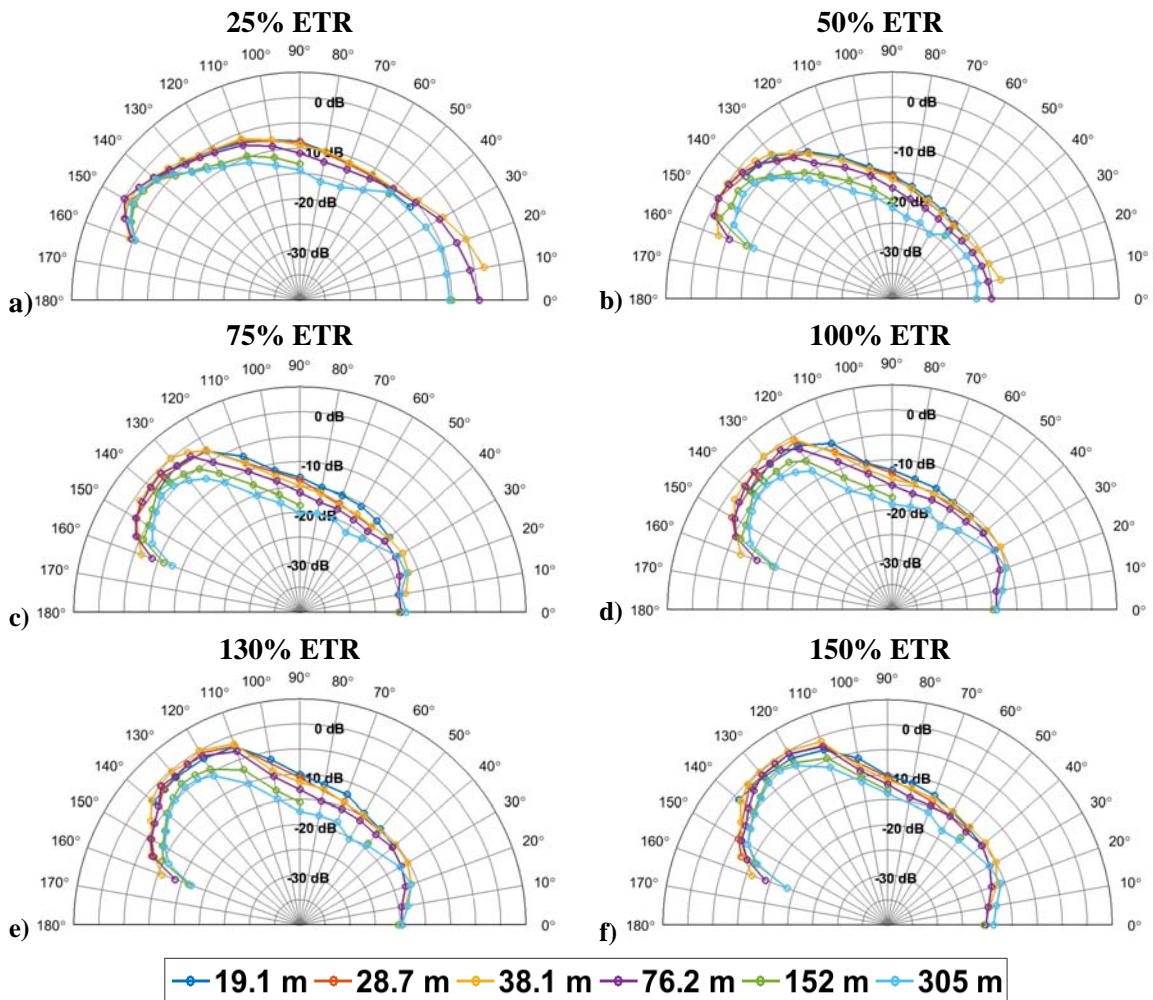
Figure 16. F-35B directivity based on normalized OASPL at distances of 19.1, 28.6, 38.1, 76.2, 152, 305 m for a) 25% ETR, b) 50% ETR, c) 75% ETR, d) 100% ETR, e) 130% ETR, and f) 150% ETR.

4. One-Third Octave Band Sound Pressure Level Normalized by Distance

The normalization process was extended to an OTO band basis to investigate changes in directivity pattern as a function of propagation distance and frequency. The overall results show similar trends as the previous results. However, one comparison for 10,000 Hz is potentially informative for evidence of nonlinear propagation. Fig. 17 compares the normalized directivities for the 10,000 Hz OTO-band-SPL for 50% and 150% ETR at distances ranging from 19.1 to 305 m. For 50% ETR, the levels are reduced as propagation distance increases as expected since atmospheric absorption is significant for this OTO band. At 305 m, the levels are 20 to 40 dB lower than the closer measurements, which is fully consistent with linear propagation. However, for 150% ETR, the 305 m levels are within 10 dB of the other distances in the maximum angular region from 110° to 160°. This comparison shows that for high engine power conditions higher frequencies are not decaying as quickly as expected with linear propagation.
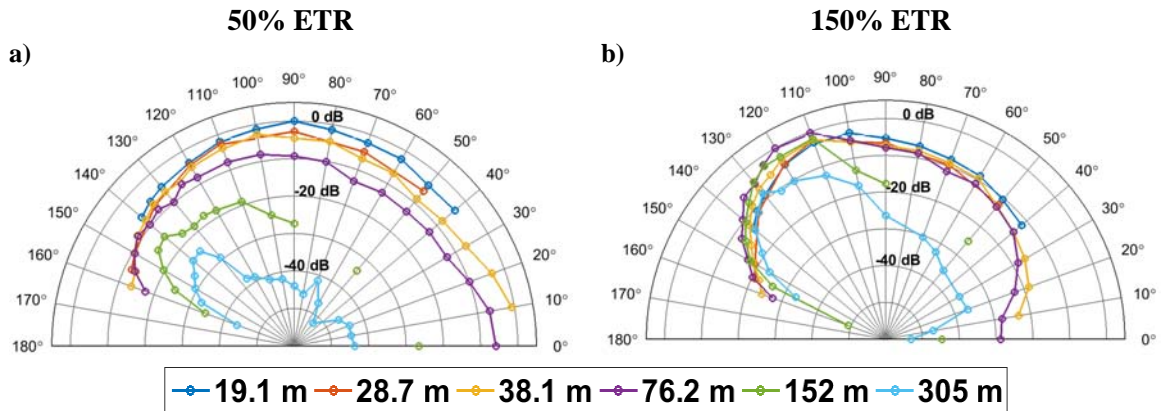
50% ETR   **150% ETR**

a)   b)

Figure 17. F-35B 10,000 Hz normalized directivity comparison between a) 50% and b) 150% ETR.

American Institute of Aeronautics and Astronautics

C. Propagation

1. One-Third Octave Band Sound Pressure Level

Additional insights regarding the nonlinearity of the propagation may be gained by comparing the measured OTO bands as a function of distance and engine power condition for a given measurement angle. Figure 18a, c, e, and g show the measured OTO band spectra for 25%, 75%, 100%, 130% ETR, respectively, along a single measurement radial at 135°. Figure 18b, d, f, and h show a comparison of the spectra normalized to 305 m by applying spherical spreading and atmospheric absorption corresponding to the atmospheric conditions during the measurements. A similar methodology was applied previously for high-performance jet aircraft noise in Refs 20, 22, and 24. For 25% ETR and 152 and 305 m, instrumentation noise floor distortion is evident at ~12,500 Hz and ~6,300 Hz, respectively. The collapse of the data up to 3150 Hz shows that good agreement exists between normalized spectra and the spectra measured at 305 m. Interference nulls around 200 Hz generate differences up to 15 dB for 152 and 305 m spectra, which occur across all engine power conditions. For engine power conditions at and above 50% ETR, the expected high-frequency roll-off from atmospheric absorption is not evident in the measured spectra at 305 m. This observation suggests nonlinear propagation is occurring since little change occurs in the slope of the high-frequency roll-off up to 305 m. For 100% and 130% ETR in Figs. 18f and h, respectively, the slope maintains an approximate 10-12 dB/decade roll-off out to 20,000 Hz at 305 m. A 10 dB/decade roll-off is physically significant because this OTO spectral decay rate results from signals, whose high-frequency content is dominated by weak shocks.[41]

The lack of an increasing spectral decay rate with distance leads to large discrepancies with spectra that assume linear atmospheric absorption. At 10,000 Hz, the differences exceed 50 dB for the 19.1 m starting point. The results of this analysis demonstrate a) a linear propagation for 25% ETR along this propagation radial, and b) the presence of significant nonlinear effects in the 75% ETR and greater engine powers, as was indicated via the derivative skewness spatial maps shown previously. The interference null at 152 and 305 m is still under investigation, but does not appear to be caused be an ordinary ground reflection; for a hard-packed dirt assumption and a point source located at the MARP, a ground reflection code based on Embleton[42] suggests the first interference null should be closer to 1 kHz. A ground with soft grass must be assumed to predict an interference null at such a low frequency, which is totally unreasonable, which suggests that the multipath effect is probably meteorology-related.

Measured
25% ETR

Normalized to 305m
25% ETR

a)

b)

50% ETR

50% ETR

c)

d)

100% ETR

100% ETR

e)

f)

130% ETR

130% ETR

g)
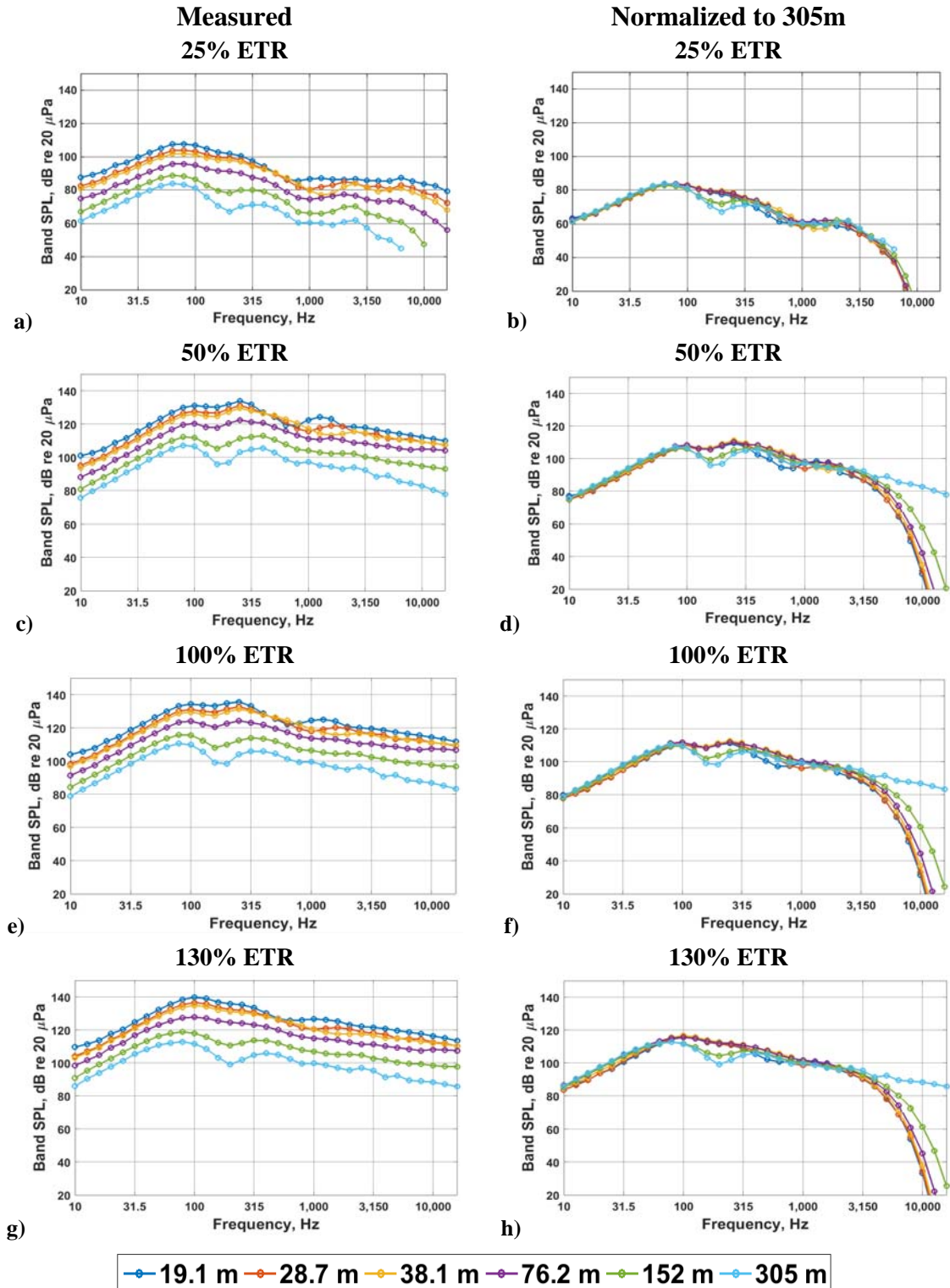
h)

19.1 m — 28.7 m — 38.1 m — 76.2 m — 152 m — 305 m

Figure 18. F-35B OTO band SPL at distances of 19.1, 28.7, 38.1, 76.2, 152, and 305 m along the 135° radial for a) 25% ETR, c) 75% ETR, e) 100% ETR, and g) 130% ETR. Propagated spectra using spherical spreading and atmospheric absorption from the measured location to 305 m for b) 25% ETR, d) 75% ETR, f) 100% ETR, and h) 130% ETR.

2. Skewness of the Pressure Derivate

In addition to comparing the spectra as a function of distance, additional insights can be gained by a comparison of the average Sk$\{\partial p/\partial t\}$ values for different engine conditions and distances. Figure 19a shows the OASPL for microphones along the 135° radial for engine conditions of 25%, 50%, 75%, 100%, 130%, and 150% ETR, as a function of distance from the MARP. As expected from the previous OASPL spatial maps, the OASPL is greater for higher ETR and decreases with distance. The decay rate in OASPL with distance is approximately 21 dB/decade, slightly more than for spherical spreading alone. More interesting than the behavior of the OASPL is that of the Sk$\{\partial p/\partial t\}$ values, shown in Figure 19b for the same locations and engine conditions. The maximum Sk$\{\partial p/\partial t\}$ value obtained is correlated with increased engine thrust. As would be expected from the discussion of Sk$\{\partial p/\partial t\}$ for Figs. 8 and 9, for engine conditions of 75% ETR and greater, the values of Sk$\{\partial p/\partial t\}$ reach a maximum at 76.2 m and then decrease with distance. Because Sk$\{\partial p/\partial t\}$ has a maximum at 76.2 m, it might be natural to assume that the shocks begin to thicken due to the presence of linear losses in the form of atmospheric absorption and geometric spreading. However, in light of the 10 dB/decade spectral roll-off seen in Fig. 18, it can be seen that the high-frequency content for 130% and 150% ETR engine powers is still essentially dominated by weak shocks at 305 m out to 20,000 Hz. This observation raises the following questions: a) what is the relationship of shock thickness with propagation distance, and b) can a metric of the waveform indicate when a waveform no longer contains weak shocks?

The weak-shock, 10 dB/decade roll-off is present in the 130% ETR shown in Fig. 18g, even at distances of 305 m and frequencies up to 20 kHz. At 75% ETR the spectra shown in Fig. 18c exhibit a similar roll-off at distances up to 152 m, but at 305 m the higher frequencies begin to roll-off at a higher rate, indicating that linear losses are beginning to thicken the shocks. Because the values of Sk$\{\partial p/\partial t\}$ begin to decrease before this change in spectral shape is evident, it can be inferred that the lower values of Sk$\{\partial p/\partial t\}$ are not necessarily indicative of shock thickening, but rather their decay in amplitude and a finite sampling rate. The decay in skewness for sawtooth waveforms with a finite sampling rate in the weak-shock regime was examined recently by Reichman *et al.*[43] However, because noise contains positive derivatives of many different values, more research is needed to estimate the strength of shocks in the waveforms, and in particular compare the strength of nonlinear effects with those of absorption and geometric spreading.
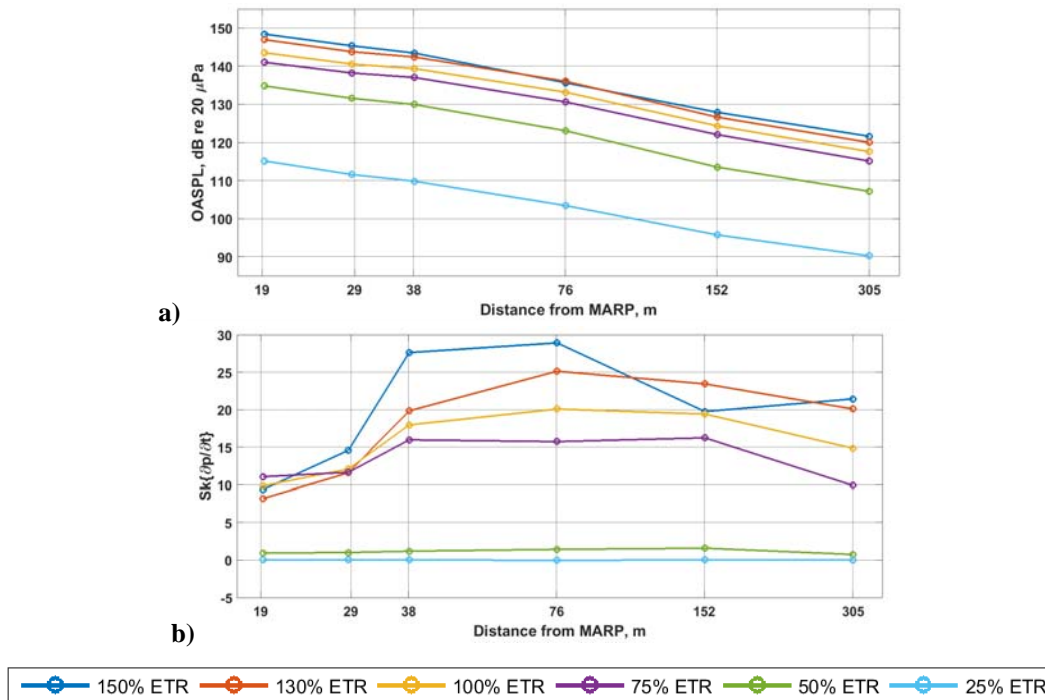

Figure 19. a) OASPL and b) skewness of pressure time derivative of F-35B as a function of distance along the 135° radial for a range of engine conditions from 25% to 150% ETR.

VI.   Conclusion

This paper includes a comprehensive analysis and discussion of the acoustic emission of an F-35B for a range of power conditions from low power to full Afterburner. The data collection procedures of ANSI/ASA S12.75 have resulted in stable acoustic data, which in turn provides consistent reference noise data for the F-35B aircraft. These reference data can be used in environmental and personnel exposure modeling and research efforts with low uncertainty from the reference data. Moreover, it has been shown that the F-35A and F-35B variants generate similar run-up noise levels. In general, the measured data follows expected trends for jet noise. However, the extent of the dataset in terms of spatial and measurement points will allow detailed analysis, which will inform jet noise models and nonlinear propagation processes.

Regarding the validation of the ANSI standard, the primary conclusions regard the MARP and the spatial sampling of the acoustic field. First, the MARP is a significant improvement, within 5° of precision, relative to the nozzle for defining directivity origins. Second, the ANSI standard should be revised to include a greater microphone density farther forward, where frequencies of critical importance radiate at high engine powers.

A number of observations have been discussed in terms of the acoustical characterization and directivity for the F-35B. First, data inside of 76.2 m for most frequencies and engine powers can be used for equivalent noise modeling without consideration for significant variation from propagation effects. Second, the invariant directivity with aircraft thrust variation of the low-frequency radiation (for 31.5 Hz and below) would appear to be of importance. Additionally, less variation was observed with thrust in the far downstream region for 100 Hz and above.

Finally, regarding propagation trends, the radiation directivity shifts forward with increase in frequency and engine power. Furthermore, the effects of engine power and frequency on nonlinear propagation versus atmospheric absorption are consistent with past studies. However, the measurement aperture allows for further insights into the statistical nature of the acoustic shocks. Nonlinear steepening explains the increase in derivative skewness, but the decay after 76.2 m needs further investigation, whether it be shock thickening or other effects, such as the nonlinear attenuation of the strongest shocks in the waveform.

References

[1] Seiner, J. M., Ukeiley, L. S., Jansen, B. J., Kannepalli, C., S. Dash, "Noise reduction technology for F/A-18E/F aircraft," AIAA Paper No. 2004-2972 (2004).

[2] Kastner, J., Heeb, N., Gutmark, E., Liu, J., & Kailasanath, K. (2012, August). Using chevrons and fluidic injection to reduce supersonic jet noise. In INTER-NOISE and NOISE-CON Congress and Conference Proceedings (Vol. 2012, No. 9, pp. 2184-2194.

[3] Kuo, C., Morris, P. J., McLaughlin, D. K., "Noise reduction in supersonic jets by nozzle fluidic inserts," AIAA Paper No. 2012-2210 (2012).

[4] Samimy, M., Kim, J.-h, Kastner, J., Adamovich, I., Utkin, Y., "Active control of high-speed and high-Reynolds-number jets using plasma actuators," J. Fluid Mech. 578, 305-330 (2007).

[5] Lighthill, M. J., "On Sound Generated Aerodynamically. I. General Theory," Royal Society of London. Series A, Mathematical and Physical Sciences 211, 1952, pp. 564-587.

[6] Hart, D. M., Neilsen, T. B., Gee, K. L., and James, M. M., "A Bayesian Based Equivalent Sound Source Model for a Military Jet Aircraft," *Proceedings of Meetings on Acoustics,* Vol. 19, Paper 055094, 2013.

[7] Mollo-Christensen, E., "Jet Noise and Shear Flow Instability Seen from an Experimenter's Viewpoint," *Journal of Applied Mechanics,* Vol. 34, 1967.

[8] Jordan, P., and Colonius, T., "Wave Packets and Turbulent Jet Noise," *Annual Review of Fluid Mechanics*, Vol. 45, 2013, pp. 173-195.

[9] Lee, S. S., and Bridges, J., "Phased-array Study of Dual-flow Jet Noise: Effect of Nozzles and Mixers," AIAA Paper 2006-2647, 2006.

[10] Schlinker, R. H., Liljenberg, S. A., Polak, D. R., Post, K. A., Chipman, C. T., and Stern, A. M., "Supersonic Jet Noise Source Characteristics & Propagation: Engine and Model Scale," AIAA Paper 2007-3623, May 2007.

[11] Harker, B. M., Gee, K. L., Neilsen, T. B., Wall, A. T., and James, M. M., "Phased-array Measurements of Full-scale Military Jet Noise," *AIAA Journal* (submitted for publication).

[12] Lee, M., and Bolton, J. S., "Source Characterization of a Subsonic Jet by Using Near-field Acoustical Holography," *Journal of the Acoustical Society of America,* Vol. 121, No. 2, 2007, pp. 967-977.

[13] Wall, A. T., Gee, K. L., Neilsen, T. B., McKinley, R. L., and James, M. M., "Military Jet Noise Source Imaging Using Multisource Statistically Optimized Near-field Acoustical Holography," *Journal of the Acoustical Society of America*, (submitted for publication).

[14] Krothapalli, A., Venkatakrishnan, L. and Lourenco, L., "Crackle: A Dominant Component of Supersonic Jet Mixing Noise," AIAA paper No. 2000-2024.

[15] Ffowcs-Williams, J. E., Simson, J. and Virchis, V. J., "'Crackle': An annoying component of jet noise," *Journal of Fluid Mechanics*, Vol. 71, No. 2., 1975, pp. 251-271.

[16] McInerny, S. A. and Olcmen, S. M., "High-intensity rocket noise: Nonlinear propagation, atmospheric absorption, and characterization," J. Acoust. Soc. Am. 117, 578-591 (2005).

[17] McInerny, S. A., "Launch vehicle acoustics Part 2: Statistics of the time domain data," J. Aircraft 33, 518-523 (1996).

[18] Morfey, C. L. and Howell, G. P., "Nonlinear Propagation of Aircraft Noise in the Atmosphere," *AIAA Journal,* Vol. 19, No. 8, 1981, pp. 986-992.

[19] Gee, K. L., Gabrielson, T. B., Atchley, A. A. and Sparrow, V. W., "Preliminary analysis of nonlinearity in military jet aircraft noise propagation," *AIAA Journal*, Vol. 43, No. 6, 2005, pp. 1398-1401.

[20] Gee, K. L., Sparrow, V. W., James, M. M., Downing, J. M., Hobbs, C. M., Gabrielson, T. B., and Atchley, A. A., "Measurement and prediction of noise propagation from a high-power jet aircraft," *AIAA Journal*, Vol. 45, No. 12, 2007, pp. 3003-3006.

[21] Saxena, S., Morris, P. J., and Viswanathan, K., "Algorithm for the Nonlinear Propagation of Broadband Jet Noise", *AIAA Journal*, Vol. 47, No. 1, 2009, pp. 186-194.

[22] Gee, K. L., Sparrow, V. W., James, M. M., Downing, J. M., Hobbs, C. M., Gabrielson, T. B., and Atchley, A. A., "The Role of Nonlinear Effects in the Propagation of Noise from High-Power Jet Aircraft," *Journal of the Acoustical Society of America*, Vol. 123, No. 6, 2008, pp. 4082-4093.

[23] McInerny, S. A., Gee, K. L. Downing, J. M., and James, M. M., "Acoustical nonlinearities in aircraft flyover data," AIAA Paper 2007-3654, May 2007.

[24] Gee, K. L., Downing, J. M., James, M. M., McKinley, R. L., McKinley, R. C., Neilsen, T. B., and Wall, A. T., "Nonlinear Evolution of Noise from a Military Jet Aircraft During Ground Run-up," AIAA Paper 2012-2258, June 2012.

[25] Gallagher, J. A. and McLaughlin, D. K., "Experiments on the Non-linear Characteristics of Noise Propagation from Low and Moderate Reynolds Number Supersonic Jets," AIAA Paper 81-2041, Oct. 1981.

[26] Petitjean, B. P. and McLaughlin, D. K. "Experiments on the Nonlinear Propagation of Noise from Supersonic Jets," AIAA Paper 2003-3127, May 2003.

[27] Gee, K. L., Neilsen, T. B., Thomas, D. C., Downing, J. M., James, M. M., and McKinley, R. L., "Comparison of two time-domain measures of nonlinearity in near-field propagation of high-power jet noise, AIAA Paper 2014-2199.

[28] Gee, K. L., Neilsen, T. B., Muhlestein. M. B., Wall, A. T., Downing, J. M., James, M. M., and McKinley, R. L., "On the Evolution of Crackle in Jet Noise from High-Performance Engines," *AIAA paper No. 2013-2190*, May 2013.

[29] Gee, K. L., Neilsen, T. B., Downing, J. M., James, M. M., McKinley, R. L., McKinley, R. C., and Wall, A. T., "Near-field Shock Formation in Noise Propagation from a High-power Jet Aircraft," *Journal of the Acoustical Society of America*, Vol. 133, 2013, EL88 – EL93.

[30] Pratt & Whitney, "Proven Power for the F-35 Lightning II – In Flight, In Production," URL: http://f135engine.com/docs/me_f135_pCard.pdf [cited 20 May 2015].

[31] Gee, K. L., Neilsen, T. B., and James, M. M., "On the crest factor of noise in full-scale supersonic jet engine measurements," Proc. Mtgs. Acoust. 20, 045003 (2014).

[32] McKinley, R. L., McKinley, R. C., Gee, K. L., Pilon, T., Mobley, F., Gillespie, M., and Downing, J. M., "Measurement of near-field and far-field noise from full scale high performance jet engines," Proc. ASME Turbo Expo 2010, Glasgow, UK, paper GT2010-22531, June 2010.

[33] Gee, K. L., Neilsen, T. B., and James, M. M., "Including source correlation and atmospheric turbulence in a ground reflection model for rocket noise," Proc. Mtgs. Acoust. **22**, 040001 (2014).

[34] Wall, A. T., Gee, K. L., Neilsen, T. B., Harker, B. M., McInerny, S. A., McKinley, R. L., and James, M. M., "Investigation of multi-lobed fighter jet noise sources using acoustical holography and partial field decomposition methods," submitted to AIAA (2015).

[35] Neilsen, T. B., Gee, K. L., and James, M. M., "Spectral characterization in the near and mid-field of military jet aircraft noise," AIAA paper 2013-2191.

[36] Stout, T. A., Gee, K. L., Neilsen, T. B., Krueger, D. W., and James , M. M., "Intensity analysis of the dominant frequencies of military jet aircraft noise," Proc. Mtgs. Acoust. 20, 040010 (2014).

[37] Tam, C. K., and Parrish, S., Noise of high-performance aircrafts at afterburner," AIAA paper No. 2014-2754 (2014).

[38] Wall, A. T., Gee, K. L., Neilsen, T. B. Kruegar, D. W., and James, M. M., "Cylindrical acoustical holography applied to full-scale jet noise," J. Acoust. Soc. Am. 136, 1120-1128 (2014).

[39] Stout, T. A., Gee, K. L., Neilsen, T. B., Wall, A. T., and James, M. M., "Acoustic intensity near a high-powered military jet aircraft, " JASA Express Letters (JASA-EL) (2015).

[40] Harker, B. M., Gee, K. L., Neilsen, T. B., Wall, A. T., James, M. M., "Phased-array measurements of full-scale military jet noise," AIAA 2014-3069.

[41] S. N. Gurbatov, O. V. Rudenko, "Statistical phenomena," chap. 13 in Nonlinear Acoustics, edited by M. F. Hamilton and D. T. Blackstock (Academic Press, San Diego, 1998), pp. 377-398.

[42] Embleton, T. W., Piercy, J. E. and Daigle, G. A., "Effective flow resistivity of ground surfaces determined by acoustical measurements," Journal of the Acoustical Society of America, vol. 74, no. 4, pp. 1239-1244, 1983.

[43] Reichman, B. O., Muhlestein, M. B., Gee, K. L., Neilsen, T. B., and Thomas, D. C., "Evolution of the time-derivative skewness of nonlinearly propagating waves," submitted to J. Acoust. Soc. Am. (2014).